Orientation dependence of inelastic scattering from the laser-excited $(\ldots 6s6p\ ^1P_1)$ state of barium

P. V. Johnson and P. W. Zetner
Department of Physics and Astronomy, University of Manitoba, Winnipeg, Manitoba, Canada R3T 2N2

D. Fursa and I. Bray
School of Physical Sciences, Flinders University of South Australia, GPO Box 2100, Adelaide 5001, Australia
(Received 16 October 2001; published 15 August 2002)

We have investigated inelastic electron scattering from the laser-excited $(\ldots 6s6p\ ^1P_1)$ state of barium at 20 eV incident electron energy and scattering angles of 5.5°, 9°, 13°, and 16°. By using circularly polarized laser light and measuring the circular polarization dependence of inelastic energy loss features associated with various excitations, we have determined the transferred orbital angular momentum parameter. L^+_{perp} for the time-inverse related deexcitations $X \rightarrow (\ldots 6s6p\ ^1P_1)$, where $X=(\ldots 6s7p\ ^1P_1)$, $(\ldots 6s6d\ ^1D_2)$, $(\ldots 6s7s\ ^1S_0)$, $(\ldots 5d^2\ ^3P_2)$ and the unresolved states $(\ldots 5d^2\ ^1D_2, \ldots 6p5d\ ^1D_2)$. Our structure calculations show some of these states to be essentially pure, two-electron states with relatively strong singlet-triplet mixing. Scattering calculations were carried out in the convergent close-coupling formalism and, in general, good agreement with experimental data is shown. A detailed analysis of the $S \rightarrow P$ and $D \rightarrow P$ deexcitations in comparison to previously reported results for $S \rightarrow P$ and $D \rightarrow P$ excitations [Y. Li and P. W. Zetner, Phys. Rev. A **49**, 950 (1994); P. V. Johnson, B. Eves, P. W. Zetner, D. Fursa, and I. Bray, Phys. Rev. A **59**, 439 (1999)] shows a selection rule of $\Delta m = +1(-1)$ to hold for excitation (deexcitation) in small-angle scattering.

DOI: 10.1103/PhysRevA.66.022707 PACS number(s): 34.80.Dp

I. INTRODUCTION

Electron collision phenomena involving excited-state atomic targets are by and large under-represented in the literature. This point was made by Trajmar and Nickel [1] in 1992 and is largely true today. Such studies present a difficult problem from both experimental and theoretical standpoints. The experimentalist is faced with the task of generating steady-state concentrations of excited-state species large enough to measure statistically significant scattering intensities. To measure scattering angle-resolved quantities, such as differential cross sections (DCS), for excited-state to excited-state processes, a substantial fraction (say, $>10\%$) of the target beam must be excited. With tuneable, cw lasers, excited-state populations of this magnitude are relatively easy to achieve, and this technique is responsible for recent progress in the field.

The application of laser excitation to collision studies restricts the target species, for the most part, to the alkali and alkaline-earth atoms with resonance transitions in a convenient (near uv to near ir) portion of the spectrum. These atomic targets are problematic for the theorist both in the determination of the target wave functions and in the approximations used in the collision model. As the atomic number Z of the target increases, electron shells underlying the valence shells can introduce electron correlation effects into the description of the wave functions, thus giving rise to a relatively complicated configuration mix. As Z increases, it is also possible that (relativistic) spin-orbit coupling effects can enter into the description of the wave function and the collisional interaction Hamiltonian. Furthermore, channel coupling effects, which are relatively small for the collisional excitation of resonance transitions at intermediate energies, can become important in the description of excited-state to excited-state scattering. Hence, first-order perturbative theories (which neglect channel coupling) may be less useful than close-coupling approaches in treating the problem.

Since the review by Trajmar and Nickel, studies of excited-state to excited-state collisions in barium and sodium have been reported [2–8]. Measurements were carried out in crossed-beam experimental configurations with momentum selection (but no spin selection) of the incident and scattered electrons. Laser radiation was tuned to the $S \rightarrow P$ resonance transitions in these atoms and scattering out of the excited P state was studied by measuring the impact energy, scattering angle and laser polarization dependence of the energy loss feature associated with the collision process of interest. In this way, the DCS for a large variety of excitations out of the Ba$(\ldots 6s6p\ ^1P_1)$ level were measured by Zetner *et al.* [4]. Additionally, population of the metastable $(\ldots 6s5d\ ^3D, ^1D)$ levels by radiative cascade from this $^1P_1$ level allowed the measurement of the DCS for excitation out of these metastable levels [5].

The use of laser radiation to generate excited atoms introduces the possibility of controlling the magnetic sublevel distribution of the target population. Generally, the distribution is anisotropic with the population of magnetic sublevel $|\mu\rangle$ being different than that of $|\mu'\rangle$ (for magnetic sublevel quantum numbers μ, μ'). Such anisotropic populations are characterized by alignment, associated with equal populations in the $|\mu\rangle$ and $|-\mu\rangle$ substates, and/or orientation, associated with unequal populations in the $|\mu\rangle$ and $|-\mu\rangle$ substates. The nature of the target population anisotropy is determined by the polarization state of the exciting laser beam. The early experiments of Hertel and collaborators [9–11] on laser-excited P-state sodium showed that electron scattering is alignment and orientation dependent. Macek and Hertel [11] developed a theoretical description in which the measured collision process (scattering from an aligned/oriented P state target) is interpreted in terms of a process related to it in a time-inverse sense (scattering that produces an aligned/oriented P state). Hence, the study of collisionally

induced transitions of the type $P \rightarrow X$ (where X represents some arbitrary, final atomic level), in which laser excitation has been used to produce an aligned/oriented P state population, allow one to ascertain the nature of collisionally induced P state alignment/orientation in the ''time-inverse'' transition $X \rightarrow P$. There has been a long history of interest in collision-induced alignment/orientation of P states and, consequently, it has become customary to describe the results of scattering studies on laser-excited P level atoms in terms of collision processes terminating on the P level. The reader is referred to the recent monograph by Andersen and Bartschat [12] for a comprehensive review of the subject.

Andersen, Gallagher, and Hertel [13] have discussed various parametrizations of the alignment and orientation of an atomic P level excited out of a (ground) S level. We refer to these various parameters as the electron impact coherence parameters (EICP). Scattering studies with laser-excited P level atoms have been carried out to determine the EICP for (ground state) $S \rightarrow P$ excitations by measuring the laser polarization dependence of scattering intensity for the inverse (superelastic) $P \rightarrow S$ deexcitation process. Such a process is completely characterized (for spin-unpolarized electrons) by four EICP and the DCS. Measurements of this type have been carried out to determine EICP for $S \rightarrow P$ transitions in sodium [9,10,14,15], lithium [16], potassium [17], rubidium [18], calcium [19], barium [20–23], ytterbium [24,25], and chromium [26].

The discussions of Andersen, Gallagher, and Hertel [13] were largely restricted to $S \rightarrow P$ transitions; however, the theory of Macek and Hertel [11] provides a simple generalization of the EICP to the case where a collisionally induced transition to the P level occurs out of an isotropically distributed magnetic sublevel population of atoms in some initial level of arbitrary total angular momentum. This generalization was described by Li and Zetner [3] and Johnson *et al.* [2] in their investigations of the (metastable) $(\ldots 6s5d\ ^1D_2) \rightarrow (..6s6p\ ^1P_1)$ inelastic transition in barium. Measurements of the DCS and four EICP for this transition were made by studying superelastic scattering for the time-inverse $P \rightarrow D$ deexcitation process. Subsequently, related measurements of generalized EICP have been reported for elastic scattering from the laser-excited $(\ldots 6s6p\ ^1P_1)$ state in barium by Trajmar *et al.* [27] and for scattering from the laser-excited $3\ ^2P$ state in sodium by Shurgalin *et al.* [6,7]. Shurgalin *et al.* measured inelastic scattering out of the $3\ ^2P$ level in sodium to determine EICP for the time inverse $4\ ^2S \rightarrow 3\ ^2P$ [6] and $3\ ^2D \rightarrow 3\ ^2P$ [7] superelastic transitions.

The present work is closely related to that of Shurgalin *et al.* in that we have studied inelastic scattering from the laser-excited $(\ldots 6s6p\ ^1P_1)$ barium state to determine one of the EICP, namely, the L^+_{perp} parameter (defined below), for the superelastic transitions $X \rightarrow (\ldots 6s6p\ ^1P_1)$ where X represents levels $(\ldots 6s7p\ ^1P_1)$, $(\ldots 6s6d\ ^1D_2)$, $(\ldots 6s7s\ ^1S_0)$, $(\ldots 5d^2\ ^3P_2)$ and the unresolved pair $(\ldots 5d^2\ ^1D_2, \ldots 6p5d\ ^1D_2)$. As noted above, measured scattering processes $P \rightarrow X$, involving an anisotropically distributed P level magnetic substate population, are described in terms of the inverse processes $X \rightarrow P$, where X represents an isotropically populated level.

This paper is organized as follows. In Sec. II we present a discussion of the measurement theory relating the measured scattering intensity to the scattering parameter of interest (L^+_{perp}). In Sec. III a brief description of the convergent close-coupling formalism is provided. In Sec. IV we describe the experimental procedure and the steps required to unfold scattering signal associated with a particular collision process from the measured energy loss spectrum. Section V presents our results with discussion, and concluding remarks are made in Sec. VI.

II. MEASUREMENT THEORY

In our earlier work [2,3], we developed the theory of Macek and Hertel to define the partial differential cross section (PDCS) for scattering out of a laser-excited $^1P_1$ state. The measured scattering signal I is proportional to the PDCS and can be written as

$$I = \kappa \sigma^{\mathrm{PDCS}}, \tag{1}$$

where κ contains factors such as detection efficiency, electron beam flux, target population and so on. The PDCS for a particular scattering process differs from the DCS in that the initial P-level population is anisotropically distributed over magnetic sublevels $|\mu\rangle$. In fact, for the laser-excited $^1P_1$ level that is of interest here, the atomic target population can be described by a wave function (i.e., it is a coherent state) which, in some reference coordinate frame, can be written as $|JN\rangle$, with $J=1$ and magnetic quantum number N. For linearly polarized laser light, an appropriate reference frame (the ''photon frame'' [10,28]) would be that in which the quantization axis lies along the oscillation direction of the optical electric field, in which case $N=0$. For circularly polarized light, an appropriate quantization axis would lie along the laser beam propagation direction (antiparallel to the beam direction in the so-called ''laser frame'' [28]) in which case $N=\pm 1$ depending on the handedness of the circular polarization. In general, the $^1P_1$ wave function can be described by a coherent (magnetic sublevel) superposition state,

$$|JN\rangle = \sum_{\mu} a_{\mu} |J\mu\rangle \tag{2}$$

for $\mu = 0, \pm 1$. The nature of this superposition is determined by the quantization axis chosen to define substates $|\mu\rangle$ and by the polarization state and incidence direction of the laser beam with respect to this quantization axis. We define the polar angles (θ_v, φ_v) of the incident laser beam with respect to the quantization axis such that the PDCS for a measured $P \rightarrow X$ scattering process (identified by its associated energy loss, ΔE) is dependent on (θ_v, φ_v) and the polarization state (which we symbolize by the letter π_v), and can be written as

$$\sigma^{\mathrm{PDCS}}(\Delta E; \theta_v, \varphi_v, \pi_v) = \frac{1}{2} \sum_{\mu_s m_s} \frac{k'}{k} \sum_{m} |\langle J' m m_s \vec{k}' | \hat{T} | JN \mu_s \vec{k} \rangle|^2. \tag{3}$$

Here $\langle J'mm_s\vec{k}'|\hat{T}|JN\mu_s\hat{k}\rangle$ is the scattering amplitude for the $P\rightarrow X$ process expressed as a matrix element of the transition operator, $\hat{T}$. It gives the amplitude for excitation of the $|J'm\rangle$ substate of level X from the laser-excited $|JN\rangle$ coherent superposition state (the $^1P_1$ state) with incident electron momentum $\vec{k}$ (spin: μ_s) and scattered electron momentum $\vec{k}'$ (spin: m_s). Substitution of Eq. (2) into Eq. (3) allows us to define the quantities

$$\rho_{ij}=\frac{\{\Sigma_m\langle J'm|\hat{T}|Ji\rangle\langle J'm|\hat{T}|Jj\rangle^*\}}{\{\Sigma_{m,\mu}|\langle J'm|\hat{T}|J\mu\rangle|^2\}}, \tag{4}$$

where the asterisk indicates a complex conjugate and the curly brackets represent the average over initial and sum over final electron spins, explicitly shown in Eq. (3). By the Macek-Hertel theory, the quantities defined in Eq. (4) are density matrix elements of the $^1P_1$ level produced by electron impact on the isotropically populated X level. The PDCS for the $P\rightarrow X$ process measured with a laser beam in polarization state π_v and incidence direction determined by (θ_v,φ_v) can thus be expressed in terms of ρ_{ij} describing the $X\rightarrow P$ process.

In this paper, we describe measurements carried out with circularly polarized laser light propagating vertically upward and striking the horizontal scattering plane perpendicularly from below. A convenient quantization axis in this case is the ''natural frame'' quantization axis described by Andersen, Gallagher, and Hertel [13] which, in our case, points along the laser beam propagation direction. Hence the angle $\theta_v=0$ (φ_v is irrelevant) and we will simplify the notation for the PDCS in Eq. (3) by eliminating θ_v and φ_v from the argument and replacing the symbol π_v with the symbol RHC (LHC) for right-hand (left-hand) circularly polarized light. With density matrix elements [Eq. (4)] defined in the natural coordinate frame, we can write

$$\sigma^{\mathrm{PDCS}}(\Delta E;\mathrm{RHC})=3\sigma^{\mathrm{DCS}}(\Delta E)\rho^n_{-1-1} \tag{5a}$$

and

$$\sigma^{\mathrm{PDCS}}(\Delta E;\mathrm{LHC})=3\sigma^{\mathrm{DCS}}(\Delta E)\rho^n_{11}, \tag{5b}$$

where the superscript n indicates natural frame density matrix elements and the quantity

$$\sigma^{\mathrm{DCS}}(\Delta E)=\frac{1}{3}\frac{k'}{k}\left\{\sum_{m,\mu}\left|\langle J'm|\hat{T}|J\mu\rangle\right|^2\right\} \tag{5c}$$

is the DCS for the measured (inelastic) collision process $P\rightarrow X$ specified by energy loss ΔE. As is evident from equation (5c), the DCS describes excitation out of an isotropic (i.e., unpolarized) $^1P_1$ level.

In the present studies of orientation dependence of $X\rightarrow P$ processes, the parameter of interest is

$$L^+_{\mathrm{perp}}=\frac{\sigma^{\mathrm{PDCS}}(\Delta E;\mathrm{LHC})-\sigma^{\mathrm{PDCS}}(\Delta E;\mathrm{RHC})}{\sigma^{\mathrm{PDCS}}(\Delta E;\mathrm{LHC})+\sigma^{\mathrm{PDCS}}(\Delta E;\mathrm{RHC})}=\frac{\rho^n_{11}-\rho^n_{-1-1}}{\rho^n_{11}+\rho^n_{-1-1}}. \tag{6}$$

This parameter, introduced by Andersen, Gallagher, and Hertel [13], gives the amount of orbital angular momentum transferred to the positive reflection symmetry component of the charge cloud in the final P state. Equivalently, the ratio $\rho^n_{11}/\rho^n_{-1-1}$, extracted from Eq. (6) once L^+_{perp} is known, gives the relative population of P-level atoms produced in the (natural frame) $\mu=\pm1$ magnetic substates by collisional deexcitation from level X. Since the upper level magnetic substates are unresolved in the measurement, the population of $\mu=\pm1$ substates is determined by an incoherent sum over squared transition amplitudes, $\langle J'm|\hat{T}|J\mu\rangle$, as is evident by rewriting Eq. (4) in the form

$$\rho^n_{ii}=\frac{k'}{3k\sigma^{\mathrm{DCS}}(\Delta E)}\sum_m|\langle J'm|\hat{T}|Ji\rangle|^2 \tag{7}$$

with $i=j=\pm1$. The arrows drawn in Fig. 1 represent the (squared) collisional transition amplitudes which couple upper level (X) magnetic substates $|m\rangle$ to P level substates $|\pm1\rangle$ for three of the levels, $X=^1S_0$, $^1P_1$, and $^1D_2$ under consideration in the present work. The assumption of conservation of reflection symmetry through the scattering plane for these singlet-singlet transitions has been made in Fig. 1. This requires that the target levels are LS coupled and that the collision Hamiltonian does not explicitly depend on the spin-orbit interaction. In the most complex transition illustrated, i.e., $^1D_2\rightarrow{}^1P_1$, conservation of reflection symmetry will reduce the number of (real) terms required in the summation in Eq. (7) from 5 to 3.

III. THE CONVERGENT CLOSE COUPLING METHOD

We have used the convergent close coupling (CCC) method to calculate the DCS and EICP for the transitions listed in Table I. Application of the CCC method to electron scattering from Ba has been extensively discussed elsewhere. We refer to Fursa and Bray [29] for a general formulation of the method and its application to electron scattering from alkaline earth atoms. The details relevant to the Ba atom have been discussed by Fursa and Bray [30] and, in Zetner *et al.* [5], it was shown how the major relativistic effect, singlet-triplet mixing in the Ba wave functions, can be taken into account in the CCC method.

In Table I we present the configuration-interaction expansions for levels included in the present study. Only major configurations were retained. The results demonstrate very strong coupling between different configurations in the wavefunctions. Two-electron configurations are very important for the description of the $(\ldots6s6p\ ^1P_1)$, $(\ldots6s7s\ ^1S_0)$, $(\ldots6s7p\ ^1P_1)$, and $(\ldots6s6d\ ^1P_1)$ levels. The $(\ldots5d^2\ ^1D_2)$, $(\ldots6p5d\ ^1D_2)$, and $(\ldots6d^2\ ^3P_2)$ levels are pure two-electron excited levels. They are very strongly affected by the breakdown of the nonrelativistic approximation which is demonstrated by large singlet-triplet mixing coefficients. Good agreement between calculated level energies and the level energies of Moore [31] is shown.

The excitation energies, relative to the $(\ldots6s6p\ ^1P_1)$ level, for all transitions studied, do not exceed 1.5 eV. The incident electron energy of 20 eV employed in the experi-

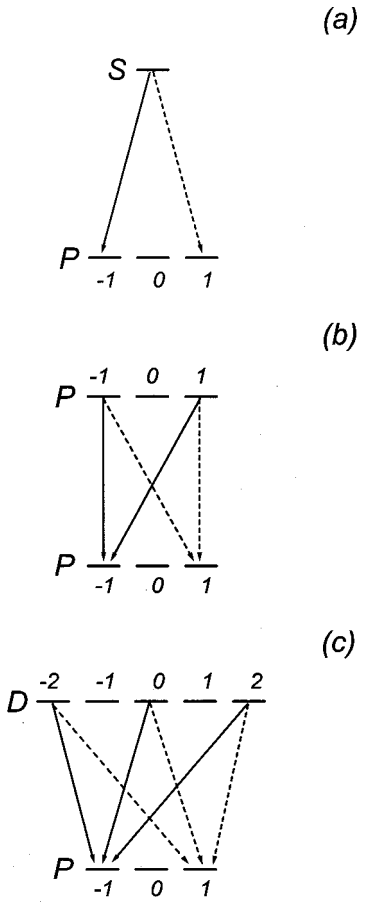

FIG. 1. Reflection symmetry-conserving superelastic scattering amplitudes for singlet transitions of the type S to P (a), P to P (b), and D to P (c). Amplitudes for transitions terminating on the $\mu = +1(-1)$ magnetic substate of the P level are represented by dashed (solid) arrows.

ments therefore corresponds to more than 13 threshold units and is close to the high-energy regime of the scattering process. Given a rather small triplet component in the $(\ldots 6s6p\ ^1P_1)$ level, we expect that, for all the transitions, the singlet-singlet, one-electron mechanism will be dominant, at least in the near-forward scattering region.

IV. EXPERIMENTAL PROCEDURE AND DATA ANALYSIS

The apparatus, an electron-energy-loss spectrometer consisting of fixed electron detector and rotatable electron gun, has been fully described by Johnson *et al.* [2] and the reader is referred to that work for details. Our measurements were carried out by developing electron-energy-loss spectra for the laser beam polarized in both right-hand and left-hand circularly polarized states. System energy resolution was approximately 90 meV at about 75 nA electron gun current and the angular resolution was about $\pm 2.5°$. Electron impact energy was calibrated on the known position of the He $2\ ^2S$ elastic scattering resonance at 19.37 eV. For this work, our focus was on the inelastic portion of the spectrum (i.e., $P \rightarrow X$ processes were of the inelastic type) and our task was to identify and isolate inelastic scattering signal corresponding to a particular $P \rightarrow X$ excitation. Equation (6) shows that only ratios of PDCS for orthogonal laser polarization states, are required to determine the L^+_{perp} parameter for the (time-inverse) superelastic $X \rightarrow P$ deexcitation. Ratios of PDCS are equal to ratios of scattering intensity [Eq. (1)] associated with a particular energy-loss feature (i.e., no normalization is required) and, hence, determination of the EICP necessitates a measurement of the polarization dependence of the scattering intensity.

Previous experiments [4,5] have shown that the inelastic portion of the energy-loss spectrum obtained from laser-excited barium vapor is highly congested with, under conditions of practical energy resolution, many overlapping features. When the laser beam and the collision interaction volume (determined by the intersection of the electron beam, vapor beam, and electron detection viewcone) overlap, the Ba vapor beam contains predominantly $(\ldots 6s^2\ ^1S_0)$, $(\ldots 6s6p\ ^1P_1)$, $(\ldots 6s5d\ ^1D_2)$, and $(\ldots 6s5d\ ^3D_2)$ species of the ^{138}Ba isotope and all other isotopes in their ground states. The conditions on atom beam collimation, laser beam intensity, and residual fields necessary to isolate the ^{138}Ba isotope for laser-pumping have been discussed by Register *et al.* [32] and are satisfied in our experiments. We refer to the geometry in which laser beam and collision interaction volume overlap as the ''laser-center'' geometry [4,5].

The laser-center geometry produces significant concentrations of $(\ldots 6s5d\ ^1D_2, ^3D_2)$ species that are metastable and electron scattering from atoms in these metastable levels contributes to the congested nature of the energy-loss spectrum. In order to isolate energy-loss features associated with $P \rightarrow X$ transitions we utilize a method developed in previous studies [4,5] where the contribution due to scattering from the D level metastables can be eliminated from a laser-center spectrum. This involves additional measurements in which the laser beam–vapor beam interaction volume is displaced upstream from the collision interaction volume. In this ''laser-low'' arrangement, target beam constituents at the collision interaction volume will comprise only ground state and D level metastables, since the short-lived P state decays in approximately 8 nsec and does not survive the transit downstream. In a sequence of steps which we will describe below, it is possible to generate an energy-loss spectrum displaying only features of the $P \rightarrow X$ type by subtracting suitably scaled versions of laser-low and laser-off (ground-state targets only) spectra from laser-center spectra.

Determination of EICP for the $X \rightarrow P$ process required us to measure the laser-polarization dependence of feature intensities corresponding to $P \rightarrow X$ inelastic scattering. Laser beam polarization was determined by a rotatable quartz phase retardation plate used in combination with a Glan-Taylor prism. The measurement was begun in the laser-center geometry. The retardation plate was rotated (by stepper motor) into the orientation required to give a desired polarization state and an energy-loss sweep over the desired energy-loss range was initiated for accumulation in a multichannel scaler (MCS). We chose the energy loss region to include the elastic scattering feature ($\Delta E = 0$) and the $^1S_0 \rightarrow {}^1P_1$ excitation feature ($\Delta E = 2.24$ eV). At the end of the sweep, the MCS provided a trigger pulse to rotate the retardation plate into the required position for the orthogonal la-

TABLE I. Level excitations out of the $6s6p\ ^1P_1$ laser-excited state studied in the present work.

Feature number[a]	Upper level: Assignment	Upper level: Dominant *LS* terms	Level excitation energy from the ground state (eV): Moore [31]	Level excitation energy from the ground state (eV): This work	Feature energy loss (eV)[b]
1	$5d^2\ ^1D_2$	$0.740(5d^2\,^1D)-0.425(5d6d\ ^1D)+0.324(6p^2\ ^1D)$ $-0.288(5d^2\ ^3P)+0.165(5d6d\ ^3P)-0.14(6p^2\ ^3P)$	2.859	3.00	0.62
1	$6p5d\ ^1D_2$	$0.834(6p5d\ ^1D)+0.427(6p5d\ ^3F)$ $-0.255(5d7p\ ^1D)-0.132(5d7p\ ^3F)$	2.861	2.87	0.622
3	$5d^2\ ^3P_2$	$0.745(5d^2\ ^3P)-0.427(5d6d\ ^3P)+0.363(6p^2\ ^3P)$ $+0.286(5d^2\ ^1D)-0.159(5d6d\ ^1D)$ $+0.126(6p^2\ ^1D)$	2.966	3.10	0.727
6	$6s7s\ ^1S_0$	$0.572(6s7s\ ^1S)-0.431(6s8s\ ^1S)+0.422(5d^2\ ^1S)$ $-0.42(5d6d\ ^1S)+0.318(6p^2\ ^1S)$	3.5	3.54	1.261
7	$6s7p\ ^1P_1$	$0.683(6s7p\ ^1P)-0.546(6p5d\ ^1P)$ $-0.329(5d7p\ ^1P)$	3.54[c]	3.60	1.301
8	$6s6d\ ^1D_2$	$0.765(6s6d\ ^1D)-0.429(6s7d\ ^1D)$ $-0.366(5d7s\ ^1D)-0.161(6d^2\ ^1D)$	3.749	3.77	1.51
	$6s6p\ ^1P_1$	$0.797(6s6p\ ^1P)-0.502(6p5d\ ^1P)$ $-0.255(6s7p\ ^1P)-0.074(6s6p\ ^3P)$	2.24	2.25	

[a]Feature numbers are those of Zetner *et al.* [4].

[b]"Feature energy loss" gives the excitation energy from the $(\ldots 6s6p\ ^1P_1)$ level. These were calculated from the values of Moore [31].

[c]Moore [31] made the assignment of $6p5d\ ^1P_1$ for this upper level.

ser polarization state and a new sweep was initiated. At the end of this sweep a sweep with laser-off was taken after which the system was reset to its starting condition. Data collection resumed in this automated fashion until laser-center spectra of suitable quality for both laser polarizations had been accumulated. Periodically, this procedure was interrupted to collect energy-loss spectra in the superelastic region. In particular, we required the $^1P_1 \rightarrow {}^1S_0$ and $^1D_2 \rightarrow {}^1S_0$ superelastic feature intensities (for both laser polarizations) in order to determine scaling factors required to combine laser-low and laser-center spectra. Laser-low spectra were then taken in the identical manner to that just described under the same experimental conditions. No superelastic spectra were required for the laser-low configuration. Measurements of this type were repeated a number of times with the selected scattering angles of 5.5°, 9°, 13°, and 16°. The scattering angle was calibrated by introducing laser light at the target which was linearly polarized along the detector axis. Superelastic $^1P_1 \rightarrow {}^1S_0$ scattering signal for this case is symmetric for scattering to the left and to the right, allowing the determination of zero degrees.

Removal of background scattering signal constituted the first step in the spectrum analysis procedure. This was accomplished by fitting a double-exponential decay to those regions of the laser-off spectra (ground state excitations) in which no features were present including the elastic tail. The fitted background function was subtracted from the laser-off spectra and the associated laser-on spectra.

The next step involved combining measured spectra, using appropriate scaling factors, to produce a final spectrum in which only features representing excitations of the type $P \rightarrow X$ were present. To proceed with our discussion of spectrum analysis, we introduce the following notation for the fractional populations of atoms (in *S*, *D*, and *P* levels) in the laser-low and laser-center geometries. In the laser-low case, we write

$$\Sigma^L = \frac{N_S^L}{N^L} \quad \text{and} \quad \Delta^L = \frac{N_D^L}{N^L}, \tag{8}$$

where the superscript "*L*" refers to laser-low and N^L, N_S^L, and N_D^L refer to the total, *S*-state and *D*-state atom populations, respectively, in the target beam. In the laser-center case, we write

$$\Sigma^C = \frac{N_S^C}{N^C}, \quad \Delta^C = \frac{N_D^C}{N^C}, \quad \text{and} \quad \Phi^C = \frac{N_P^C}{N^C}, \tag{9}$$

where the "*C*" superscript refers to laser center and N^C, N_S^C, N_D^C, and N_P^C refer to the total, *S*-state, *D*-state, and *P*-state atom populations, respectively, in the target beam.

In the above notation N_D^L and N_D^C refer to the combined population of $(\ldots 6s5d\ ^1D_2, {}^3D_2)$ metastables. The fractional populations are constrained by the equations

$$\Sigma^L + \Delta^L = 1 \tag{10a}$$

and

$$\Sigma^C + \Delta^C + \Phi^C = 1. \tag{10b}$$

With these quantities defined, we can write the feature intensities in our measured (background-subtracted) energy-loss spectra as

$$I^L(\Delta E) = C^L N^L [\Sigma^L \sigma_S^{\mathrm{DCS}}(\Delta E) + \Delta^L \sigma_D^{\mathrm{DCS}}(\Delta E)], \tag{11a}$$

$$I^L_{\mathrm{off}}(\Delta E) = C^L N^L \sigma_S^{\mathrm{DCS}}(\Delta E), \tag{11b}$$

$$I^C(\Delta E;\pi_v) = C^C N^C [\Sigma^C \sigma_S^{\mathrm{DCS}}(\Delta E) + \Delta^C \sigma_D^{\mathrm{DCS}}(\Delta E) + \Phi^C \sigma_P^{\mathrm{PDCS}}(\Delta E;\pi_v)], \tag{11c}$$

$$I^C_{\mathrm{off}}(\Delta E) = C^C N^C \sigma_S^{\mathrm{DCS}}(\Delta E), \tag{11d}$$

where the superscript $L(C)$ refers to laser-low (laser-center), the subscripts S, D, and P denote cross sections involving initial ground-state, D-state, and P-state atoms, respectively, and the constants C^C, C^L involve factors such as electron beam flux, detection efficiency and so on (exclusive of target atom population) which relate the measured intensities to the cross sections. The symbol π_v refers to the polarization state of the laser light. Note that, in Eqs. (11a)-(11c), we have assumed scattering from the D-level target atoms to be described by a DCS (isotropic target) as opposed to a PDCS (anisotropic target). In principle, the D states can be aligned/oriented since they are populated by radiative cascade from an aligned/oriented P state. However, our studies have revealed no measurable laser-polarization dependence of scattering from the D states in both the laser-low and laser-center geometries. These conclusions are based on the subtraction of spectra taken with orthogonal polarizations in both of these geometries. A discussion of systematic effects responsible for disalignment of the D states is given by Zetner *et al.* [5]. Equations (11a)–(11d) suggest the appropriate combination of scaled spectra to give an energy-loss spectrum, $I_P(\Delta E;\pi_v)$, of features associated only with $P \rightarrow X$ excitations,

$$I_P(\Delta E;\pi_v) = C^C N^C \Phi^C \sigma_P^{\mathrm{PDCS}}(\Delta E;\pi_v). \tag{12}$$

This result can be obtained by combining the measured spectra according to

$$I_P(\Delta E;\pi_v) = I^C(\Delta E;\pi_v) - \Sigma^C I^C_{\mathrm{off}}(\Delta E) - \frac{C^C N^C}{C^L N^L}\frac{\Delta^C}{\Delta^L}[I^L(\Delta E) - \Sigma^L I^L_{\mathrm{off}}(\Delta E)]. \tag{13}$$

The scaling factors appearing in Eq. (13) can be generated using the measured intensities of certain energy-loss features. For example,

$$\frac{C^C N^C}{C^L N^L} = \frac{I^C_{\mathrm{off}}\ (2.24\ \mathrm{eV})}{I^L_{\mathrm{off}}\ (2.24\ \mathrm{eV})}, \tag{14}$$

where the intensities are those associated with the ground state $^1S_0 \rightarrow {}^1P_1$ inelastic feature at energy loss $\Delta E = 2.24$ eV. The fractional populations Σ^C and Σ^L are approximately given by

$$\Sigma^L = \frac{I^L\ (2.24\ \mathrm{eV})}{I^L_{\mathrm{off}}\ (2.24\ \mathrm{eV})} \tag{15}$$

and

$$\Sigma^C = \frac{I^C\ (2.24\ \mathrm{eV};\pi_v)}{I^C_{\mathrm{off}}\ (2.24\ \mathrm{eV})}. \tag{16}$$

The validity of Eqs. (15), (16) rests on the assumption that the intensity of features corresponding to $P \rightarrow X$ and $D \rightarrow X'$ excitations which underlie the (ground) $^1S_0 \rightarrow {}^1P_1$ feature can be neglected, i.e.,

$$\Sigma^L \sigma_S^{\mathrm{DCS}}\ (2.24\ \mathrm{eV}) \gg \Delta^L \sigma_D^{\mathrm{DCS}}\ (2.24\ \mathrm{eV}), \tag{17a}$$

$$\Sigma^C \sigma_S^{\mathrm{DCS}}\ (2.24\ \mathrm{eV}) \gg \Delta^C \sigma_D^{\mathrm{DCS}}\ (2.24\ \mathrm{eV}), \tag{17b}$$

and

$$\Sigma^C \sigma_S^{\mathrm{DCS}}\ (2.24\ \mathrm{eV}) \gg \Phi^C \sigma_P^{\mathrm{PDCS}}\ (2.24\ \mathrm{eV};\pi_v). \tag{17c}$$

The appearance of the symbol π_v in Eqs. (16) and (17c) indicate that the approximation is taken to hold for both laser beam polarization states. In our experiments, the approximations (17a)-(17c) appeared to be well satisfied, consistent with observations made by Zetner *et al.* [4,5].

The last scaling factor required in Eq. (13) is the ratio of D-state fractional populations in the laser-center and laser-low geometries. Using Eqs. (8)–(10) we can express this ratio as

$$\frac{\Delta^C}{\Delta^L} = \frac{(1-\Sigma^C)}{(1-\Sigma^L)}\left(1 + \frac{\Phi^C}{\Delta^C}\right)^{-1}. \tag{18}$$

We determined this ratio by measuring signal intensities (in the laser-center geometry) for the well-resolved $(\ldots 6s6p\ {}^1P_1) \rightarrow (\ldots 6s^2\ {}^1S_0)$ and $(\ldots 6s5d\ {}^1D_2) \rightarrow (\ldots 6s^2\ {}^1S_0)$ superelastic transitions at energy losses of $\Delta E = -2.24$ and -1.41 eV, respectively. The ratio of these feature intensities (measured in the same spectrum) is

$$\frac{I^C\ (-2.24\ \mathrm{eV};\pi_v)}{I^C\ (-1.41\ \mathrm{eV};\pi_v)} = \frac{N^C_P}{N^C_{^1D_2}}\frac{\sigma_P^{\mathrm{PDCS}}\ (-2.24\ \mathrm{eV};\pi_v)}{\sigma^{\mathrm{DCS}}_{^1D_2}\ (-1.41\ \mathrm{eV})}. \tag{19}$$

The validity of Eq. (19) rests on two assumptions. First, the instrumental detection efficiency is assumed to be the same at the two energy-loss values (-2.24 and -1.41 eV). Second, the averaging effect on the scattering signal due to the spatial distribution of scatterers through the collision volume is assumed to be the same for excited-state $^1P_1$ and $^1D_2$ atoms. The first assumption rests on the fact that the separation, in energy loss, between the two features is small (0.83 eV) in comparison to the incident electron energy (20 eV) and the focal properties of the electron optics remain constant over this range, as previous work with this instrument has shown. The second assumption is less well justified as the rate equation modeling of excited-state populations [33]

shows different spatial distributions for atoms in the D and $^1P_1$ levels within the collision volume. While the $^1P_1$ population is nearly symmetrically distributed with respect to the center of the laser beam intensity profile (assumed Gaussian), the D level atoms, because of their metastable character, are very asymmetrically distributed with a population that takes on a constant, maximum value downstream of the laser beam center. Consequently, scattering from the D level atoms, asymmetrically distributed within the 5° detection viewcone, is weighted somewhat toward scattering angles different from the nominal scattering angle defined by the central axis of the detection viewcone. The relationship between measured scattering intensity and the cross section for a scattering process under conditions of finite instrumental resolution (in energy and angle) is discussed in detail by Brinkmann and Trajmar [34]. For our purposes, the error introduced by differently distributed scatterers lies in employing the DCS for $^1D_2 \rightarrow {}^1S_0$ deexcitation [in the denominator of Eq. (19)] for the nominal scattering angle. We expect this error to be relatively small in relation to some of the other errors discussed in this section. From Eq. (19), it is clear that the ratio $N_P^C/N_{^1D_2}^C$ can be calculated if the PDCS for the $^1P_1 \rightarrow {}^1S_0$ deexcitation and the DCS for the $^1D_2 \rightarrow {}^1S_0$ deexcitation are known. The relationship between this ratio and the desired ratio of fractional populations required in Eq. (18) is

$$\frac{\Phi^C}{\Delta^C} = 0.7 \frac{N_P^C}{N_{^1D_2}^C}. \tag{20}$$

The factor of 0.7 arises from the branching fractions of Bizzari and Huber [35] which shows that radiative cascade produces a total D-level population comprising 70% $^1D_2$ and 30% $^3D_2$ population (with a negligible $^3D_1$ component).

The PDCS for $^1P_1 \rightarrow {}^1S_0$ deexcitation and the DCS for $^1D_2 \rightarrow {}^1S_0$ deexcitation required in Eq. (19) were obtained from the DCS for the inverse (excitation) processes, $^1S_0 \rightarrow {}^1P_1$ and $^1S_0 \rightarrow {}^1D_2$ reported by Jensen, Register, and Trajmar [36]. The relationship between the DCS for time-inverse processes is given by the principle of detailed balance. Specifically, the DCS for the $P \rightarrow X$ transition (impact energy E_0) is related to the DCS for the $X \rightarrow P$ process (impact energy $E_0 - \Delta E$) by

$$[\sigma_{P\rightarrow X}^{\mathrm{DCS}}(\Delta E)]_{E_0} = \left(\frac{g_x}{g_p}\right)\left(\frac{E_0 - \Delta E}{E_0}\right)[\sigma_{X\rightarrow P}^{\mathrm{DCS}}(-\Delta E)]_{E_0-\Delta E}, \tag{21}$$

where g_X and g_P are level degeneracies of the X and P levels, respectively ($g_P = 3$). We made a small approximation in utilizing this equation. Our present measurements were carried out at 20 eV impact energy. Hence, Eq. (21) relates the (superelastic) DCS for $^1P_1 \rightarrow {}^1S_0$ deexcitation at 20 eV impact energy to the (inelastic) DCS for $^1S_0 \rightarrow {}^1P_1$ excitation at 17.76 eV impact energy. Likewise, the (superelastic) DCS for $^1D_2 \rightarrow {}^1S_0$ deexcitation at 20 eV impact energy is related to the (inelastic) DCS for $^1S_0 \rightarrow {}^1D_2$ excitation at 18.59 eV impact energy. Our approximation involved using the 20 eV impact energy DCS of Jensen, Register, and Trajmar [36] for the $^1S_0 \rightarrow {}^1P_1$ and $^1S_0 \rightarrow {}^1D_2$ excitation processes. We note that the 20 eV $^1S_0 \rightarrow {}^1P_1$ DCS data of Jensen, Register, and Trajmar [36] is in excellent agreement with the more recent measurements of Wang, Trajmar, and Zetner [37]. To convert the DCS for the $^1P_1 \rightarrow {}^1S_0$ process to the PDCS required in Eq. (19), we used the L_{perp}^+ parameters for the $^1S_0 \rightarrow {}^1P_1$ transition reported by Li and Zetner [20]. For this transition it was found that $\rho_{00}^n = 0$ in which case

$$\rho_{11}^n = 1 - \rho_{-1-1}^n = \tfrac{1}{2}(L_{\mathrm{perp}}^+ + 1) \tag{22}$$

and the PDCS can be obtained from Eq. (5) in conjunction with the DCS. Rigorously the L_{perp}^+ parameters for 17.76 eV impact energy are required in the PDCS determination whereas the utilized parameters were measured at 20 eV impact energy.

V. RESULTS AND DISCUSSION

Figure 2 shows a representative $P \rightarrow X$ excitation spectrum produced by scaling and combining laser-low and laser-center spectra (with their associated laser-off spectra) according to Eq. (13). Spectrum fitting with a Gaussian line-shape function enabled us to extract feature intensities associated with excitations ($\ldots 6s6p\ ^1P_1$) to X for levels X listed in Table I. Analysis of the (circular) polarization dependence of the feature intensities allowed the determination of L_{perp}^+ parameters for the time-inverse X (isotropic) to ($\ldots 6s6p\ ^1P_1$) deexcitations. The measured results are tabulated in Table II and plotted in the figures below along with the results of the CCC calculations and the CCC calculations convoluted with the finite collision interaction volume. Details of this convolution procedure are given by Zetner, Trajmar, and Csanak [28] and Zetner, Li, and Trajmar [21]. Error limits on the experimental data were obtained from the uncertainties in the spectral line fitting coefficients (amplitudes of the Gaussian line shape) returned by the fitting routine.

Figure 3 shows the L_{perp}^+ parameter extracted from the polarization dependence of feature 1 (Table I). This is a blended feature corresponding to two unresolved transitions in which the final levels are an even and an odd parity $^1D_2$ state arising from the (dominant) two-electron configurations $5d^2$ and $6p5d$, respectively. Table I gives the results of structure calculations which show that the ($\ldots 5d^2\ ^1D_2$) level contains an admixture (11%) of $^3P_2$ and the ($\ldots 6s5d\ ^1D_2$) level contains an admixture (20%) of $^3F_2$. The feature displayed a weak polarization dependence that gives an L_{perp}^+ parameter in fair agreement with CCC results. Theoretical results for the blended feature were obtained by calculating the PDCS in Eqs. (5a), (5b) for the individual transitions, summing the PDCS and generating L_{perp}^+ by using the summed values in Eq. (6). Alternatively, one can show that the L_{perp}^+ parameter for a blended transition with two components can be expressed in terms of the individual parameters, $L_{\mathrm{perp}}^+(1)$ and $L_{\mathrm{perp}}^+(2)$, as

$$L_{\mathrm{perp}}^+ = L_{\mathrm{perp}}^+(1)\cos^2\xi + L_{\mathrm{perp}}^+(2)\sin^2\xi, \tag{23}$$

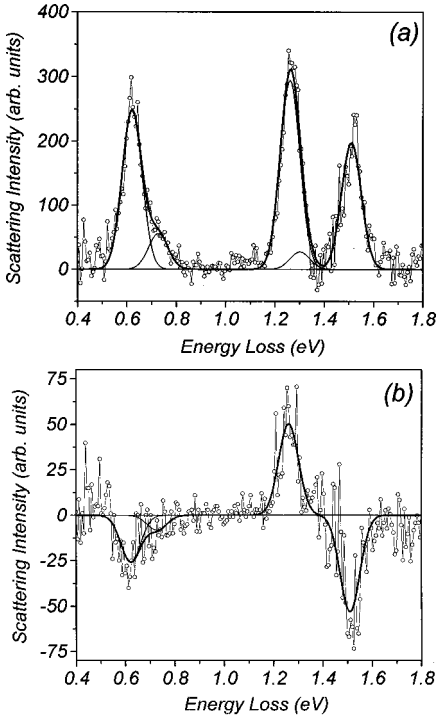

FIG. 2. Measured and fitted spectra for $(\ldots 6s6p\ ^1P_1)$ to X transitions at 5.5° scattering angle and 20 eV incident electron energy. Measured spectra obtained with right-hand and left-hand circularly polarized light were combined to form the sum spectrum (a) and the difference spectrum (b). The five features listed in Table I were fitted using Gaussian line shapes of equal width and the energy-loss values given in Table I. Composite synthetic spectra (bold curves) and individual line shapes are shown.

where

$$\tan^2\xi = \frac{\sigma^{\mathrm{DCS}}(2)}{\sigma^{\mathrm{DCS}}(1)}\frac{(1-\rho_{00}^n(2))}{(1-\rho_{00}^n(1))}.$$

The "blended" L_{perp}^+ parameter consists of weighted contributions from the two unresolved transitions where the weighting factors involve the DCS for the individual transitions $[\sigma^{\mathrm{DCS}}(1)$ and $\sigma^{\mathrm{DCS}}(2)]$ as well as the corresponding natural frame density matrix elements $\rho_{00}^n(1)$ and $\rho_{00}^n(2)$. The ρ_{00}^n matrix element is also called the "height parameter" h and takes on values in the range $0 \leqslant h \leqslant 0.5$ [13]. With

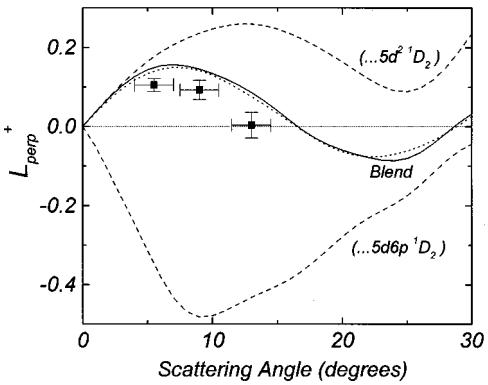

FIG. 3. The L_{perp}^+ parameter for deexcitation of the unresolved $(\ldots 5d^2\ ^1D_2, \ldots 5d6p\ ^1D_2)$ levels to the $(\ldots 6s6p\ ^1P_1)$ level at 19.4 eV impact energy. Measured data are represented by solid squares with error bars. The solid curve is the result of the CCC calculation while the dotted curve represents a finite interaction volume modeling calculation employing the CCC results. Calculated CCC results for transitions out of the individual $(\ldots 5d^2\ ^1D_2)$ and $(\ldots 5d6p\ ^1D_2)$ levels are also presented (dashed curves).

labels "1" and "2" referring to the $5d6p\ ^1D_2$ and $5d^2\ ^1D_2$ levels, respectively, comprising the blend, theoretical predictions of $\tan^2\xi$ in the CCC formalism give values of 18.17, 6.84, and 2.97 at scattering angles of 5.5°, 9°, and 13°, respectively. We note also that calculated DCS ratios for excitation of the $5d^2\ ^1D_2$ level relative to the $5d6p\ ^1D_2$ level are 18.32, 7.11, and 3.12 at scattering angles 5.5°, 9°, and 13°, respectively, which shows, upon comparison with $\tan^2\xi$, that the DCS, and not the h parameter, determines the behavior of the blended L_{perp}^+ parameter at small angles. Clearly, the $5d^2\ ^1D_2$ component dominates in near-forward scattering and consequently, to a good approximation, we expect the measured L_{perp}^+ parameter at 5.5° to describe the $(\ldots 5d^2\ ^1D_2)$ to $(\ldots 6s6p\ ^1P_1)$ deexcitation. The CCC calculations of L_{perp}^+ for the resolved transitions are also plotted in Fig. 3. It is interesting to note the radical dissimilarity in the angular behavior of L_{perp}^+ predicted by the CCC theory for the two component transitions of the unresolved feature. Over the range of scattering angles $0 \leqslant \theta \leqslant 30°$, the sign of L_{perp}^+ is predicted to be opposite. The agreement between measured and theoretical results for the blended feature, with L_{perp}^+ values greater than zero, indirectly supports the CCC prediction

TABLE II. Measured L_{perp}^+ parameters for the superelastic processes $X \rightarrow (\ldots 6s6p\ ^1P_1)$.

Level X	Electron impact energy (eV)	Scattering angle (deg)[a]			
		5.5	9	13	16
$5d^2\ ^1D_2$ $6p5d\ ^1D_2$ (blend)	19.4	0.11(0.02)	0.09(0.02)	0.00(0.03)	
$5d^2\ ^3P_2$	19.3	0.15(0.04)	0.17(0.06)	0.17(0.09)	
$6s7s\ ^1S_0$	18.7	−0.17(0.02)	−0.27(0.06)	−0.73(0.25)	
$6s6d\ ^1D_2$	18.5	0.17(0.02)	0.24(0.03)	0.18(0.04)	0.06(0.04)
$6s7p\ ^1P_1$	18.7	−0.03(0.23)	−0.04(0.12)	0.07(0.1)	

[a]Quantities in parentheses represent the measurement uncertainties.

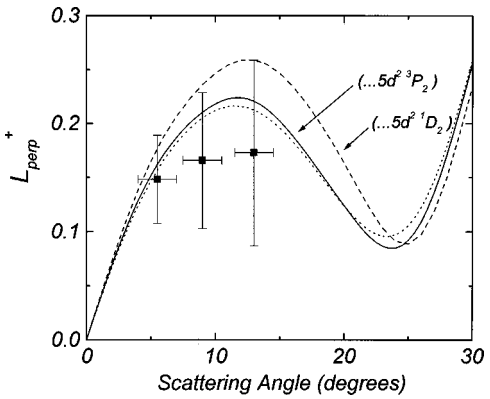

FIG. 4. The $L^+_{\rm perp}$ parameter for deexcitation of the $(\ldots 5d^2\ ^3P_2)$ level to the $(\ldots 6s6p\ ^1P_1)$ level at 19.3 eV impact energy. The measured data are represented by solid squares with error bars. The solid curve is the result of the CCC calculation while the dotted curve represents a finite interaction volume modeling calculation employing the CCC results. Calculated CCC results for the transition out of the $(\ldots 5d^2\ ^1D_2)$ level are also presented (dashed curve) for comparison.

that the $(\ldots 6s6p\ ^1P_1)$ to $(\ldots 5d^2\ ^1D_2)$ excitation is much stronger than the $(\ldots 6s6p\ ^1P_1)$ to $(\ldots 5d6p\ ^1D_2)$ excitation in near-forward scattering. It is also interesting to note that, in the first Born approximation, amplitudes for two-electron transitions between the configurations $5d^2\ ^1D_2$ and $6s6p\ ^1P_1$ are zero. Also, amplitudes for the one-electron, dipole-forbidden transition between configurations $5d6p\ ^1D_2$ and $6s6p\ ^1P_1$ are small in the forward scattering region, where dipole-allowed transitions dominate. However, the $(\ldots 5d^2\ ^1D_2)$ level has a substantial admixture of the $(\ldots 6p^2\ ^1D_2)$ configuration while the $(\ldots 6s6p\ ^1P_1)$ level has a significant contribution from the $(\ldots 6p5d\ ^1P_1)$ configuration. Hence, the dipole-allowed transitions $(\ldots 6p^2\ ^1D_2) \rightarrow (\ldots 6s6p\ ^1P_1)$ and $(\ldots 5d^2\ ^1D_2) \rightarrow (\ldots 6p5d\ ^1P_1)$ likely dominate the scattering at the small angles and relatively high-impact energy studied here.

Figure 4 gives our results for the $(\ldots 5d^2\ ^3P_2)$ to $(\ldots 6s6p\ ^1P_1)$ deexcitation. A good agreement between experiment and theory is shown. According to the structure calculations, the upper, even parity, $^3P_2$ level is predominantly triplet P in nature (87%) but contains an admixture of $^1D_2$ (12%) including the $(\ldots 6p^2\ ^1D_2)$ configuration (1.6%). We also show CCC results for the $(\ldots 5d^2\ ^1D_2) \rightarrow (\ldots 6s6p\ ^1P_1)$ transition in Fig. 4. The remarkable similarity in $L^+_{\rm perp}$ behavior predicted by CCC calculations for the $(\ldots 5d^2\ ^1D_2) \rightarrow (\ldots 6s6p\ ^1P_1)$ and $(\ldots 5d^2\ ^3P_2) \rightarrow (\ldots 6s6p\ ^1P_1)$ transitions reinforces the suggestion made above that the dipole-allowed, $(\ldots 6p^2\ ^1D_2) \rightarrow (\ldots 6s6p\ ^1P_1)$ and $(\ldots 5d^2\ ^1D_2) \rightarrow (\ldots 6p5d\ ^1P_1)$ components of the transition play the dominant role in each case.

Figure 5(a) shows the $L^+_{\rm perp}$ parameter for the $(\ldots 6s7s\ ^1S_0) \rightarrow (\ldots 6s6p\ ^1P_1)$ superelastic (deexcitation) process. This is a one-electron $s \rightarrow p$ transition that is dipole allowed. The agreement between measurements and theory is good for this case. The small-angle behavior of this parameter is very similar to the characteristic behavior of $^1S_0 \rightarrow {}^1P_1$ excitations observed for many targets and collision

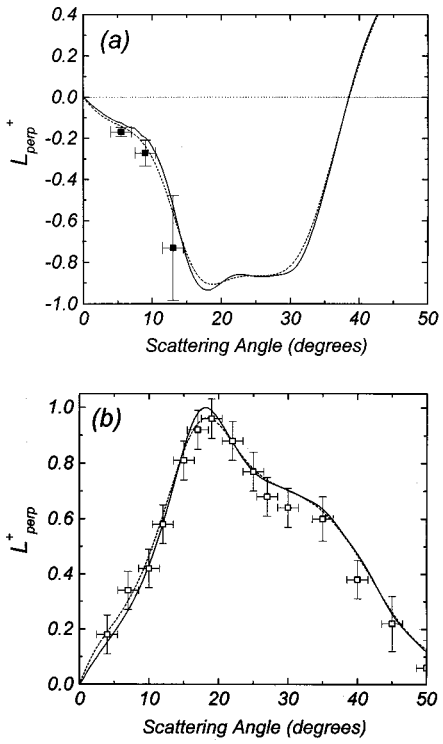

FIG. 5. (a) The $L^+_{\rm perp}$ parameter for deexcitation of the $(\ldots 6s7s\ ^1S_0)$ level to the $(\ldots 6s6p\ ^1P_1)$ level at 18.7 eV impact energy. The measured data are represented by solid squares with error bars. The solid curve is the result of the CCC calculation while the dotted curve represents a finite interaction volume modeling calculation employing the CCC results. (b) The $L^+_{\rm perp}$ parameter for deexcitation of the $(\ldots 6s6p\ ^1P_1)$ level out of the $(\ldots 6s^2\ ^1S_0)$ level at 36.7 eV impact energy. Measured data from Li and Zetner [20] are represented by open squares with error bars. The solid curve is the result of the CCC calculation while the dotted curve represents a finite interaction volume modeling calculation employing the CCC results.

energies but with inverted sign. In fact, comparison of the present data (collision energy of 14.8 threshold units) with our previous studies [20] of the $(\ldots 6s^2\ ^1S_0) \rightarrow (\ldots 6s6p\ ^1P_1)$ excitation at 36.7 eV (collision energy of 16.4 threshold units), reproduced in Fig. 5(b), reveals this similarity most convincingly. The sign is opposite but, in both cases, $|L^+_{\rm perp}|$ increases smoothly to a peak value of unity near 20° scattering angle and then begins to decrease. This observation is completely consistent with the propensity rule proposed by Andersen and Hertel [38] to relate $L^+_{\rm perp}$ measured in $s \rightarrow p$ excitation to the corresponding measurement in $s \rightarrow p$ deexcitation. Propensity rules have been discussed further by Bartschat, Andersen, and Loveall [39] and Andersen and Bartschat [12] with specific reference to the experiment on sodium carried out by Shurgalin *et al.* [6,40]. Shurgalin *et al.* determined the $L^+_{\rm perp}$ parameter for the $3s \rightarrow 3p$ excitation process (22 eV collision energy) and $4s \rightarrow 3p$ deexcitation process (25.2 eV collision energy) in sodium to find significantly different angular behavior of $|L^+_{\rm perp}|$. The propensity rule was shown to hold only over a very restricted angular range in the near-forward regime. Bartschat, Andersen, and Loveall [39] tied this behavior to

the large polarizability of the $4s$ state (due to strong coupling of the $4s$ state to states other than $3p$) and the consequent importance of partial waves with high angular momentum in the collision through the long-range polarization interaction. Application of the conclusions of Bartschat, Andersen, and Loveall [39] with the demonstrated validity of the propensity rule in the present work suggests that partial waves of high angular momentum do not dominate the collisional interaction in the kinematic regime studied.

Figure 6(a) gives results for the $(\ldots 6s6d\ ^1D_2) \rightarrow (\ldots 6s6p\ ^1P_1)$ deexcitation that is, largely, a dipole-allowed, one-electron $d \rightarrow p$ transition (see Table I). The agreement between measurement and theory is good at 5.5° and 9° but becomes somewhat less satisfactory at other angles. While theoretical results show a significant peak near 12°, measured data suggest a somewhat smaller maximum. The present result for a $D \rightarrow P$ deexcitation are compared with previous data of Johnson *et al.* [2] for the $(\ldots 6s5d\ ^1D_2) \rightarrow (\ldots 6s6p\ ^1P_1)$ excitation, reproduced in Fig. 6(b). The 10 eV impact energy data of Johnson *et al.* [2], corresponding to 12.0 times the threshold excitation energy, was chosen to compare with the present 18.5 eV impact energy results (12.2 times the threshold excitation energy). The observations show that the sign of $L^+_{\rm perp}$ in small angle scattering is opposite for the two $D \rightarrow P$ transitions and, hence, the propensity rule governing the sign change of $L^+_{\rm perp}$ for excitation versus deexcitation processes appears to hold for transitions more complex than the simple $S \rightarrow P$ case.

A comparison of Figs. 5 and 6 shows that, in small-angle scattering, the $D \rightarrow P$ transitions are characterized by $L^+_{\rm perp}$ parameters opposite in sign to the $S \rightarrow P$ transitions (in both excitation and deexcitation). Examination of Fig. 1 prompted us to consider whether the common feature in the $D \rightarrow P$ and $S \rightarrow P$ transitions responsible for the observed sign change is the predominance of transition amplitudes for $\Delta m = \mu - m = +1(-1)$ in excitation (deexcitation). This is obviously true in the $S \rightarrow P$ cases to produce the observed sign of $L^+_{\rm perp}$ but, if the argument is applied to the $D \rightarrow P$ cases it requires the squared amplitudes $|\langle {}^1D_2(m=-2)|\hat{T}|{}^1P_1(\mu=-1)\rangle|^2$ and $|\langle {}^1D_2(m=2)|\hat{T}|{}^1P_1(\mu=1)\rangle|^2$ to dominate in excitation and deexcitation, respectively. This requirement arises because there is an additional $\Delta m = +1(-1)$ amplitude in excitation (deexcitation) describing transitions originating on the $^1D_2$ $(m=0)$ substate and terminating on the $^1P_1(\mu)$ substate of opposite angular momentum to the one preferentially excited (to give the observed sign of $L^+_{\rm perp}$). Calculated natural-frame CCC amplitudes (squared) are plotted in Fig. 7. Calculations indicate that amplitudes for reflection symmetry-nonconserving transitions are zero and, as Fig. 7 shows, the dominant amplitudes in small-angle scattering are $\langle {}^1D_2(m=-2)|\hat{T}|{}^1P_1(\mu=-1)\rangle$ in excitation and $\langle {}^1D_2(m=2)|\hat{T}|{}^1P_1(\mu=-1)\rangle$ in deexcitation. Note that this result is consistent with optical transition probabilities that favor the $^1D_2(m=\pm 2) \rightarrow {}^1P_1(m=\pm 1)$ transitions over the $^1D_2(m=0) \rightarrow {}^1P_1(m=\pm 1)$ transitions by a factor of 6. In fact, this factor of 6 is evident in the ratio of calculated amplitudes for forward scattering. To further illustrate the similarities in the

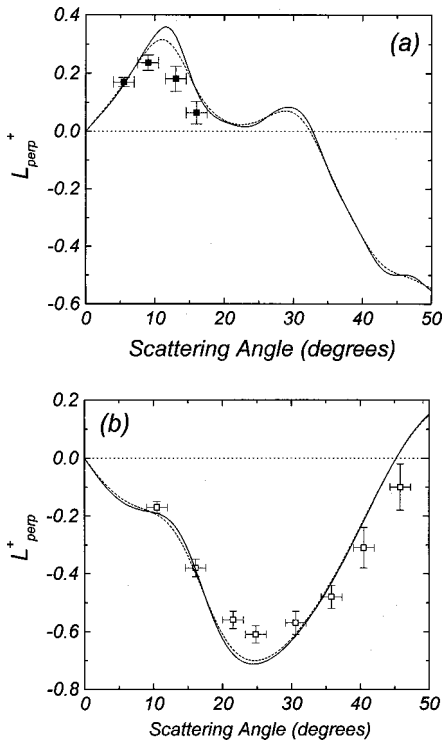

FIG. 6. (a) The $L^+_{\rm perp}$ parameter for deexcitation of the $(\ldots 6s6d\ ^1D_2)$ level to the $(\ldots 6s6p\ ^1P_1)$ level at 18.5 eV impact energy. Measured data are represented by solid squares with error bars. The solid curve is the result of the CCC calculation while the dotted curve represents a finite interaction volume modeling calculation employing the CCC results. (b) The $L^+_{\rm perp}$ parameter for excitation of the $(\ldots 6s6p\ ^1P_1)$ level out of the $(\ldots 6s5d\ ^1D_2)$ level at 10.0 eV impact energy. Measured data from Johnson *et al.* [2] are represented by open squares with error bars. The solid curve is the result of the CCC calculation while the dotted curve represents a finite interaction volume modeling calculation employing the CCC results.

$S \rightarrow P$ and $D \rightarrow P$ processes, we have combined the calculated CCC amplitudes to generate summed amplitudes for $\Delta m = \pm 1$ (and $\Delta m = \pm 3$ in the $D \rightarrow P$ case) transitions and present the results in Fig. 8. A very strong resemblance in the small-angle behavior of the amplitudes for $S \rightarrow P$ and $D \rightarrow P$ scattering is observed with a ''selection rule'' for dominant $\Delta m = +1(-1)$ transitions evident in the excitation (deexcitation) case. These observations suggest that the propensity rule of Andersen and Hertel [38] can be generalized to link the sign of Δm to the sign of the momentum transfer for these optically allowed transitions.

Finally, Fig. 9 shows the behavior of $L^+_{\rm perp}$ for the one-electron, dipole-forbidden $(\ldots 6s7p\ ^1P_1) \rightarrow (\ldots 6s6p\ ^1P_1)$ deexcitation. This transition was somewhat more difficult to analyze than those discussed above because of the proximity of the associated energy-loss feature to the stronger $(\ldots 6s7s\ ^1S_0) \rightarrow (\ldots 6s6p\ ^1P_1)$ feature (see Fig. 2). However, some qualitative agreement between the CCC theory and the experiment is shown. Relatively little is known about $P \rightarrow P$ transitions, therefore further study is warranted, particularly in view of the interesting structures predicted for the $L^+_{\rm perp}$ parameter, such as the pronounced and rather sharp

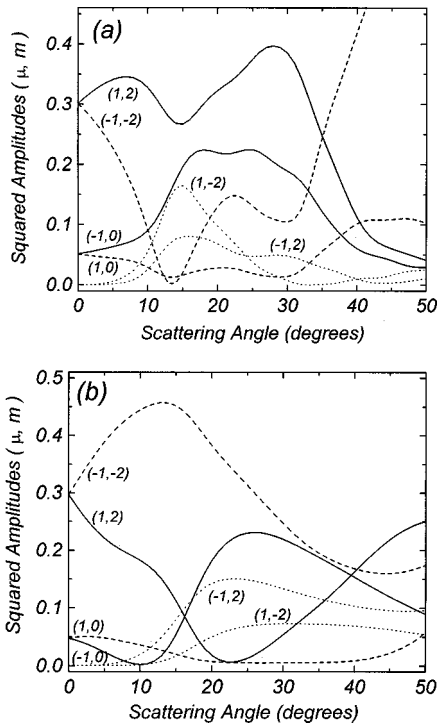

FIG. 7. Natural frame, squared, CCC transition amplitudes for (a) the $(\ldots 6s6d\ ^1D_2)$ to $(\ldots 6s6p\ ^1P_1)$ superelastic transition at 18.5 eV impact energy and (b) the $(\ldots 6s5d\ ^1D_2)$ to $(\ldots 6s6p\ ^1P_1)$ inelastic transition at 10.0 eV impact energy. Amplitudes coupling the D-level substate with magnetic quantum number m to the P-level substate with magnetic quantum number μ are identified by the ordered pair (μ,m). The amplitudes have been normalized so that the sum over all m and μ of their squares is set equal to unity. Solid (dashed, dotted) curves indicate $\Delta m=-1(+1,\pm 3)$ transitions.

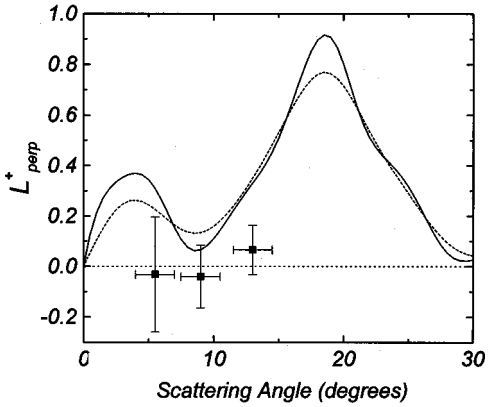

FIG. 9. The $L^+_{\rm perp}$ parameter for deexcitation of the $(\ldots 6s7p\ ^1P_1)$ level to the $(\ldots 6s6p\ ^1P_1)$ level at 18.7 eV impact energy. The measured data are represented by solid squares with error bars. The solid curve is the result of the CCC calculation while the dotted curve represents a finite interaction volume modeling calculation employing the CCC results.

peak near 18° shown in Fig. 9. We note that elastic scattering on the laser-excited $(\ldots 6s6p\ ^1P_1)$ state has been investigated by Trajmar *et al.* [27] which, in principle, bears some resemblance to $P\rightarrow P$ inelastic scattering. Their work did not utilize oriented P-state atoms and hence no comparison is made with our results.

VI. CONCLUSIONS

We have presented measurements and CCC calculations of the $L^+_{\rm perp}$ parameter for the deexcitation $X \rightarrow (\ldots 6s6p\ ^1P_1)$ where $X=(\ldots 6s7p\ ^1P_1)$, $(\ldots 6s6d\ ^1D_2)$, $(\ldots 6s7s\ ^1S_0)$, $(\ldots 5d^2\ ^3P_2)$ and the unresolved levels $(\ldots 5d^2\ ^1D_2, \ldots 6p5d\ ^1D_2)$. In general, a good agreement

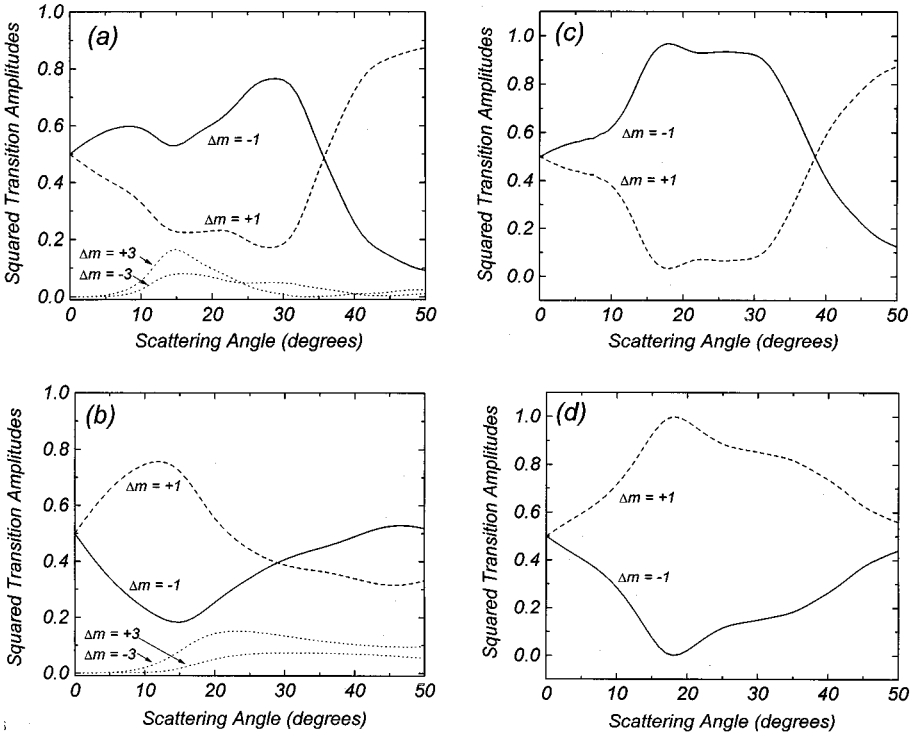

FIG. 8. Sums over squared, natural-frame CCC transition amplitudes satisfying the conditions; $\Delta m=\mu-m=-1$ (solid curves), $+1$ (dashed curves), and ± 3 (dotted curves) for (a) $(\ldots 6s6d\ ^1D_2)$ to $(\ldots 6s6p\ ^1P_1)$ deexcitation at 18.5 eV impact energy, (b) $(\ldots 6s5d\ ^1D_2)$ to $(\ldots 6s6p\ ^1P_1)$ excitation at 10.0 eV impact energy, (c) $(\ldots 6s7s\ ^1S_0)$ to $(\ldots 6s6p\ ^1P_1)$ deexcitation at 18.7 eV impact energy, and (d) $(\ldots 6s^2\ ^1S_0)$ to $(\ldots 6s6p\ ^1P_1)$ excitation at 36.7 eV impact energy.

between experiment and theory is demonstrated for both dipole-allowed and dipole-forbidden transitions. A good agreement is also shown for cases in which there is rather substantial singlet-triplet mixing [i.e., the $(\ldots 5d^2\ ^1D_2)$, $(\ldots 6p5d\ ^1D_2)$, and $(\ldots 5d^2\ ^3P_2)$ states] although, at the small angles and large impact energy (relative to the excitation energies of transitions involving these states) studied here, we would expect the collisional interaction to be dominated by singlet-singlet scattering. It would be desirable to carry out studies at the lower impact energy, where the triplet component of the initial state plays a more important role, to further test the capabilities of the theory. A detailed analysis of the $S \rightarrow P$ and $D \rightarrow P$ deexcitations, and of previous results for the $S \rightarrow P$ and $D \rightarrow P$ excitations, shows a selection rule of $\Delta m = +1(-1)$ to hold in excitation (deexcitation) at small scattering angles and suggests a generalization of the Andersen-Hertel propensity rule to more complicated transitions.

ACKNOWLEDGMENTS

Financial support by the Natural Sciences and Engineering Research Council of Canada, as well as the University of Manitoba, is gratefully acknowledged by P. V. Johnson and P. W. Zetner. These authors also wish to thank S. Trajmar and I. Kanik at the Jet Propulsion Laboratory, Pasadena, California, for a continuing equipment loan. Support by the Australian Research Council and the Flinders University of South Australia is acknowledged by D. Fursa and I. Bray, who also wish to express their indebtedness to the South Australia Center for High Performance Computing and Communications.

[1] S. Trajmar and J. C. Nickel, Adv. At., Mol., Opt. Phys. **30**, 45 (1992).
[2] P. V. Johnson, B. Eves, P. W. Zetner, D. Fursa, and I. Bray, Phys. Rev. A **59**, 439 (1999).
[3] (a) Y. Li and P. W. Zetner, J. Phys. B **28**, 5151 (1995); (b) **29**, 1803 (1996).
[4] P. W. Zetner, S. Trajmar, S. Wang, I. Kanik, G. Csanak, R. E. H. Clark, J. Abdallah, Jr., and J. C. Nickel, J. Phys. B **30**, 5317 (1997).
[5] P. W. Zetner, S. Trajmar, I. Kanik, S. Wang, G. Csanak, R. E. H. Clark, J. Abdallah, Jr., D. Fursa, and I. Bray, J. Phys. B **32**, 5123 (1999).
[6] M. Shurgalin, A. J. Murray, W. R. MacGillivray, M. C. Standage, D. H. Madison, K. D. Winkler, and I. Bray, J. Phys. B **32**, 2434 (1999).
[7] M. Shurgalin, A. J. Murray, W. R. MacGillivray, and M. C. Standage, J. Phys. B **31**, 4205 (1998).
[8] T. Y. Jiang, Z. Shi, C. H. Ying, L. Vuskovic, and B. Bederson, Phys. Rev. A **51**, 3773 (1995).
[9] H. W. Hermann, I. V. Hertel, W. Reiland, A. Stamatovic, and W. Stoll, J. Phys. B **10**, 251 (1977).
[10] I. V. Hertel and W. Stoll, Adv. At. Mol. Phys. **13**, 1113 (1977).
[11] J. Macek and I. V. Hertel, J. Phys. B **7**, 2173 (1974).
[12] N. Andersen and K. Bartschat, *Polarization, Alignment and Orientation in Atomic Collisions* (Springer-Verlag, New York, 2001).
[13] N. Andersen, J. W. Gallagher, and I. V. Hertel, Phys. Rep. **165**, 1 (1988).
[14] R. T. Sang, P. M. Farrell, D. H. Madison, W. R. MacGillivray, and M. C. Standage, J. Phys. B **27**, 1187 (1994).
[15] R. E. Scholten, S. R. Lorentz, J. McClelland, M. H. Kelly, and R. J. Celotta, J. Phys. B **24**, L653 (1991).
[16] V. Karaganov, I. Bray, and P. J. O. Teubner, Phys. Rev. A **59**, 4407 (1999).
[17] K. A. Stockman, V. Karaganov, I. Bray, and P. J. O. Teubner, J. Phys. B **32**, 3003 (1999).
[18] B. V. Hall, M. Shurgalin, A. J. Murray, W. R. MacGillivray, and M. C. Standage, Aust. J. Phys. **52**, 515 (1999).
[19] M. R. Law and P. J. O. Teubner, J. Phys. B **28**, 2257 (1995).
[20] Y. Li and P. W. Zetner, Phys. Rev. A **49**, 950 (1994).
[21] (a) P. W. Zetner, Y. Li, and S. Trajmar, J. Phys. B **25**, 3187 (1992); (b) P. W. Zetner, Y. Li, and S. Trajmar, Phys. Rev. A **48**, 495 (1993).
[22] P. V. Johnson, C. Spanu, Y. Li, and P. W. Zetner, J. Phys. B **33**, 5367 (2000).
[23] P. V. Johnson, C. Spanu, and P. W. Zetner, J. Phys. B **34**, 4311 (2001).
[24] Y. Li and P. W. Zetner, J. Phys. B **27**, L293 (1994).
[25] P. W. Zetner, P. V. Johnson, Y. Li, G. Csanak, R. E. H. Clark, and J. Abdallah, Jr., J. Phys. B **34**, 1619 (2001).
[26] G. F. Hanne, J. J. McClelland, R. E. Scholten, and R. J. Celotta, J. Phys. B **26**, L753 (1993).
[27] S. Trajmar, I. Kanik, M. A. Khakoo, L. R. LeClair, I. Bray, D. Fursa, and G. Csanak, J. Phys. B **32**, 2801 (1999).
[28] P. W. Zetner, S. Trajmar, and G. Csanak, Phys. Rev. A **41**, 5980 (1990).
[29] D. V. Fursa and I. Bray, J. Phys. B **30**, 5895 (1997).
[30] D. V. Fursa and I. Bray, Phys. Rev. A **59**, 282 (1999).
[31] C. Moore, *Atomic Energy Levels as Derived from Analysis of Optical Spectra*, Natl. Bur. Stand. (US), Circ. No. 467 (US GPO, Washington, DC, 1958).
[32] D. F. Register, S. Trajmar, G. Csanak, S. W. Jensen, M. A. Fineman, and R. T. Poe, Phys. Rev. A **28**, 151 (1983).
[33] P. V. Johnson, Ph.D. thesis, University of Manitoba, Canada, 1999 (unpublished).
[34] R. T. Brinkmann and S. Trajmar, J. Phys. E **14**, 245 (1981).
[35] A. Bizzarri and M. C. E. Huber, Phys. Rev. A **42**, 5422 (1990).
[36] S. Jensen, D. Register, and S. Trajmar, J. Phys. B **11**, 2367 (1978).
[37] S. Wang, S. Trajmar, and P. W. Zetner, J. Phys. B **27**, 1613 (1994).
[38] N. Andersen and I. V. Hertel, Comments At. Mol. Phys. **19**, 1 (1986).
[39] K. Bartschat, N. Andersen, and D. Loveall, Phys. Rev. Lett. **83**, 5254 (1999).
[40] M. Shurgalin, A. J. Murray, W. R. MacGillivray, M. C. Standage, D. H. Madison, K. D. Winkler, and I. Bray, Phys. Rev. Lett. **81**, 4604 (1998).